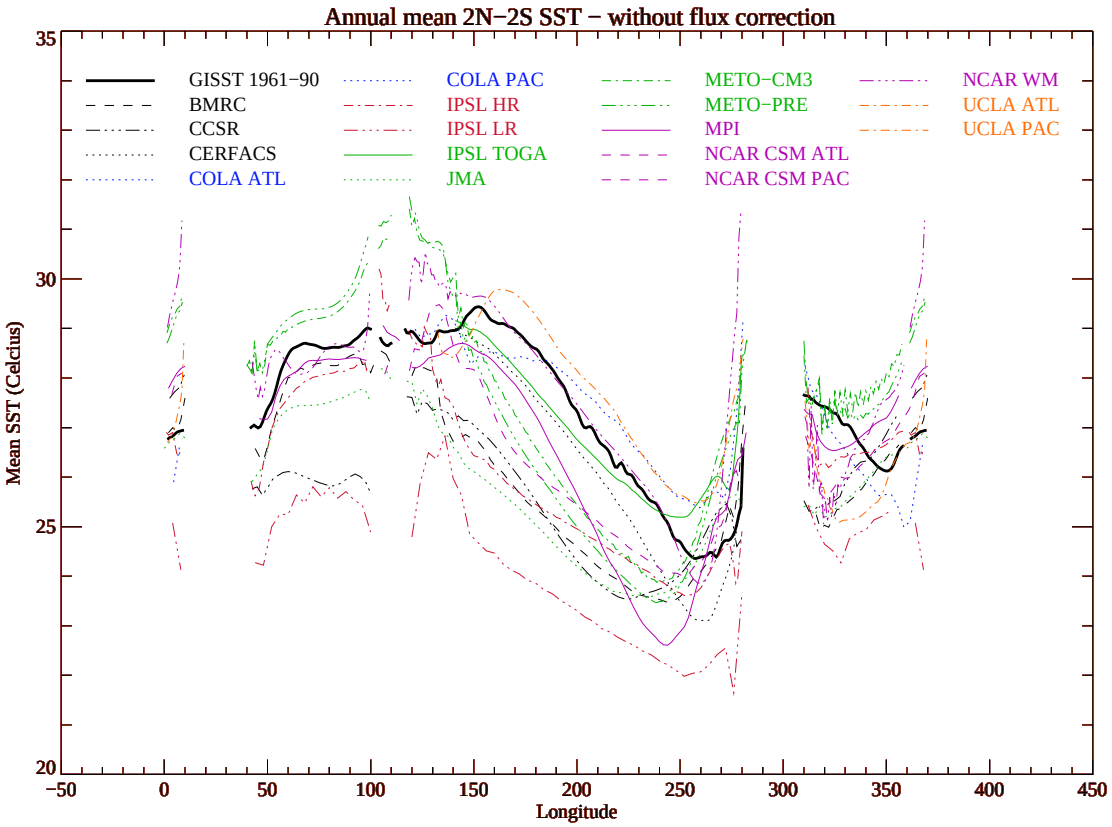

Figure 1.0.1 Annual mean SST zonal section for equatorial strip 2N-2S, as observed and for non-flux corrected CGCMs (with permission of M. Davey, see Davey et al 2002)

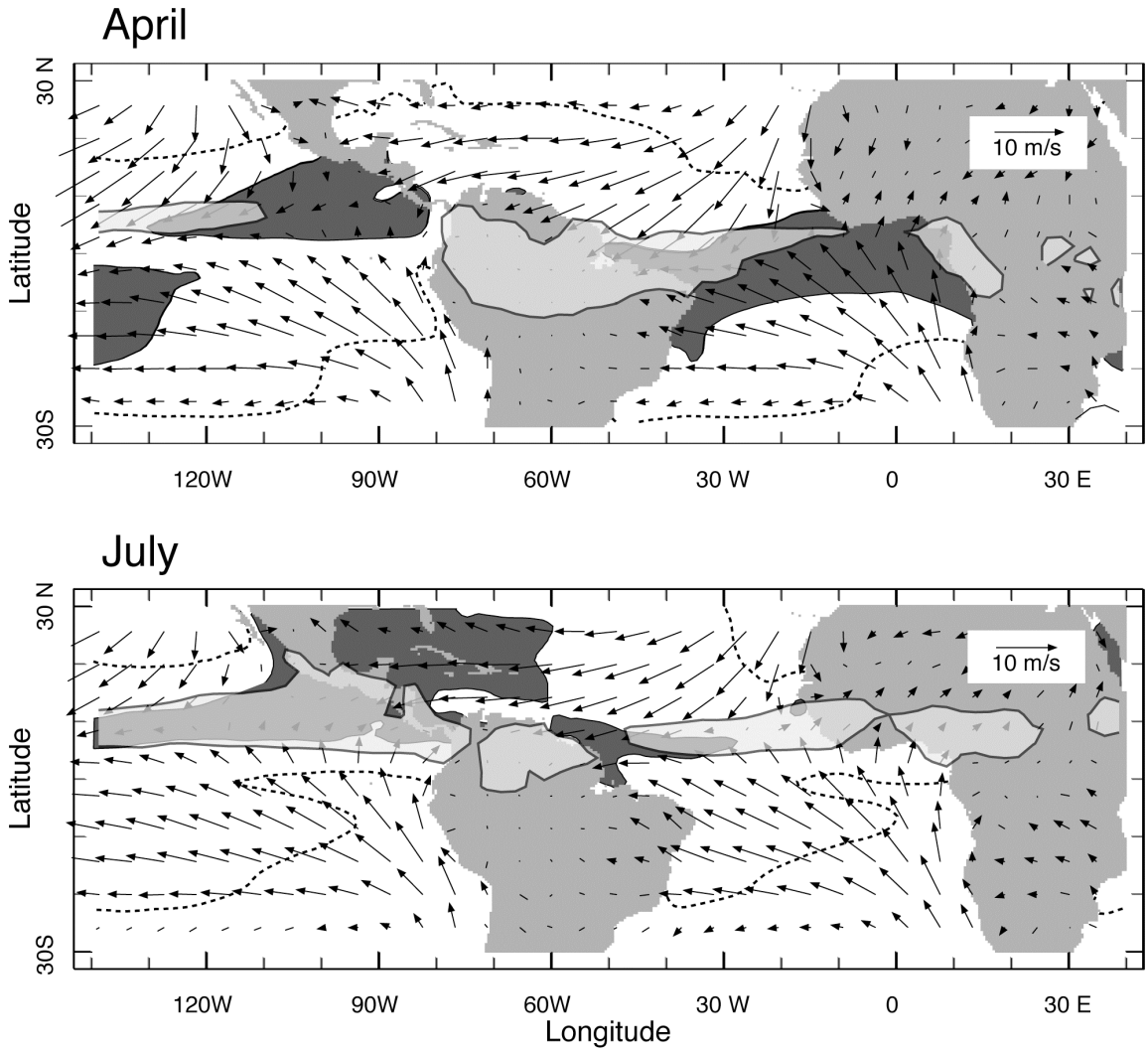

Figure 1.1.1a April and July climatologies of the tropical Atlantic and eastern Pacific. Dark shaded areas are regions with SST ≥28°C. Light, semi-transparent areas are regions with rainfall ≥6 mm/day (the ITCZ). The arrows depict the surface (10 m) wind vectors with scale indicated in the figure. The dotted contour is the 24°C isotherm demarking the regions of relatively cold water and the eastern ocean cold tongues. SST and wind data are from NCEP/NCAR CDAS-1 (Reanalysis) and rainfall from GPCP.

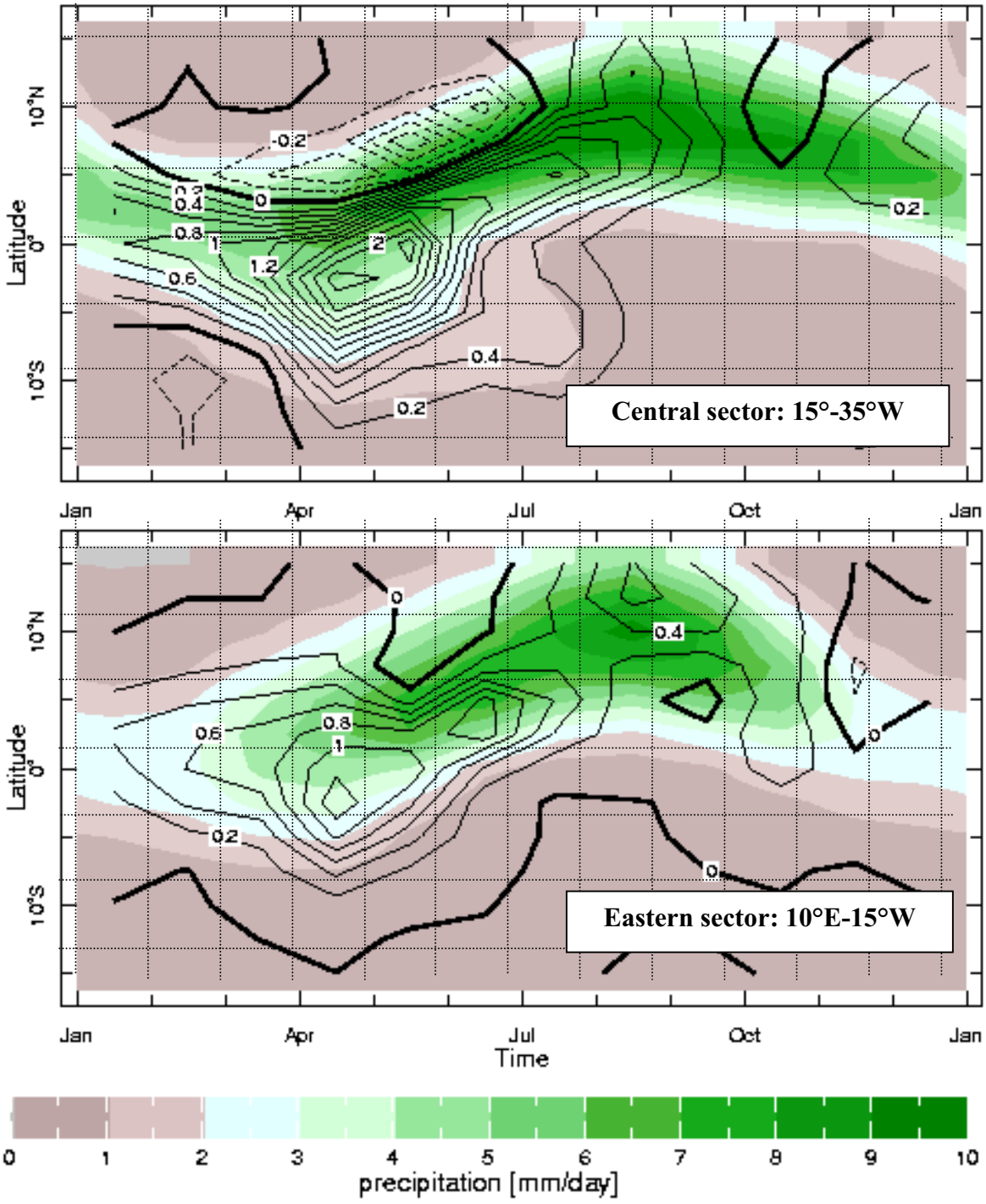

Figure 1.1.1b Annual migration of the Atlantic marine ITCZ as depicted in two longitude-sector averages (indicated on figure) climatological mean rainfall (in mm/day, see color scale) as a function of the calendar month (abscissa) and latitude (ordinate). Also shown is the first EOF of the variability around the climatology in the latitude – calendar month space (also in mm/day). Data are from the NASA GPCP (Hofman et al., 1997) spanning the years 1999-2001.

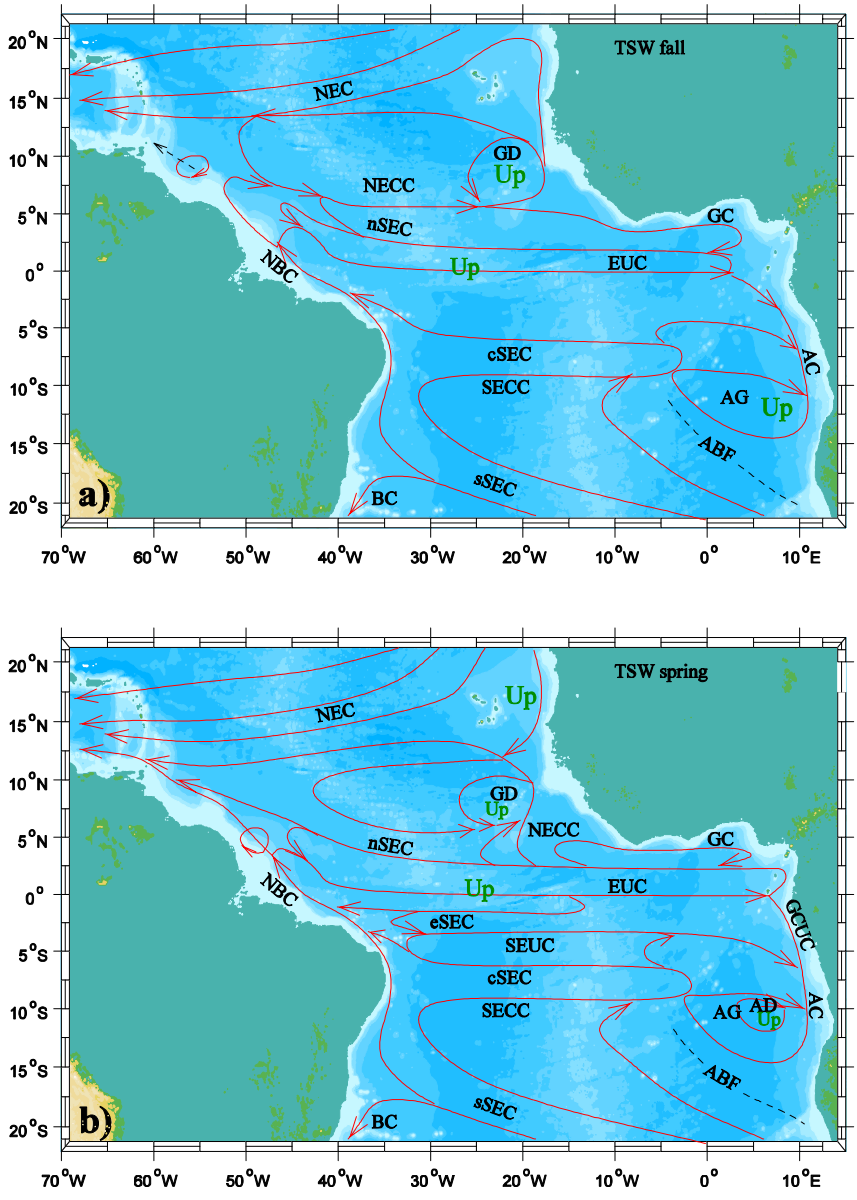

Figure 1.1.2 Schematic maps showing the horizontal distribution of the major tropical currents for the Tropical Surface Water layer at about 0-100 m depth for a) the northern spring and for b) the northern fall. Shown are the North Equatorial Current (NEC), the Guinea Dome (GD), the North Equatorial Countercurrent (NECC), the Guinea Current (GC), the South Equatorial Current (SEC) with the northern (nSEC), equatorial (eSEC), central (cSEC) and southern branches (sSEC), the Equatorial Undercurrent (EUC), the North Brazil Current (NBC), the Gabon-Congo Undercurrent (GCUC), the Angola Gyre (AG), the Angola Current (AC), the Angola Dome (AD), the South Equatorial Undercurrent (SEUC), the South Equatorial Countercurrent (SECC) and the Brazil Current (BC). The Angola-Benguela Front (ABF) is included as a dashed line. "Up" marks possible areas of upwelling, but not the exact places (see also Fig 1.5.2); (from Stramma et al., 2003).

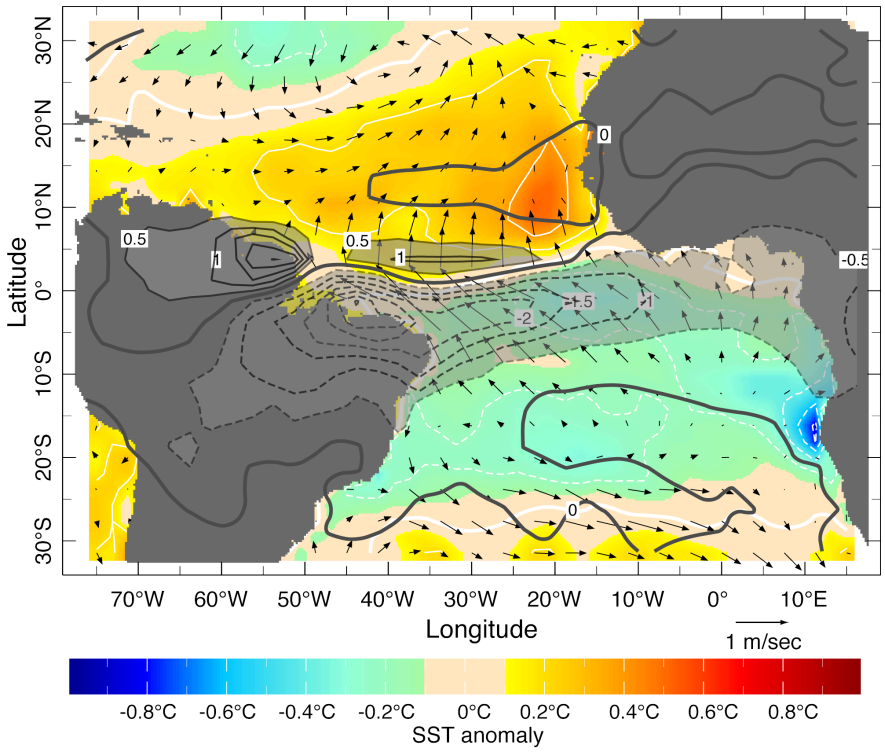

Figure 1.1.3a: Typical boreal spring variability in the tropical Atlantic region presented in terms of the first EOF (explains 33% of the variance) of March-April rainfall from GPCP 1979-2001 (contours in mm/day). The March-April SST anomaly (colors, in °C & white contours, every 0.2°) and surface wind anomaly (vector, in m/sec) are determined through regression on the time series of the rainfall EOF.

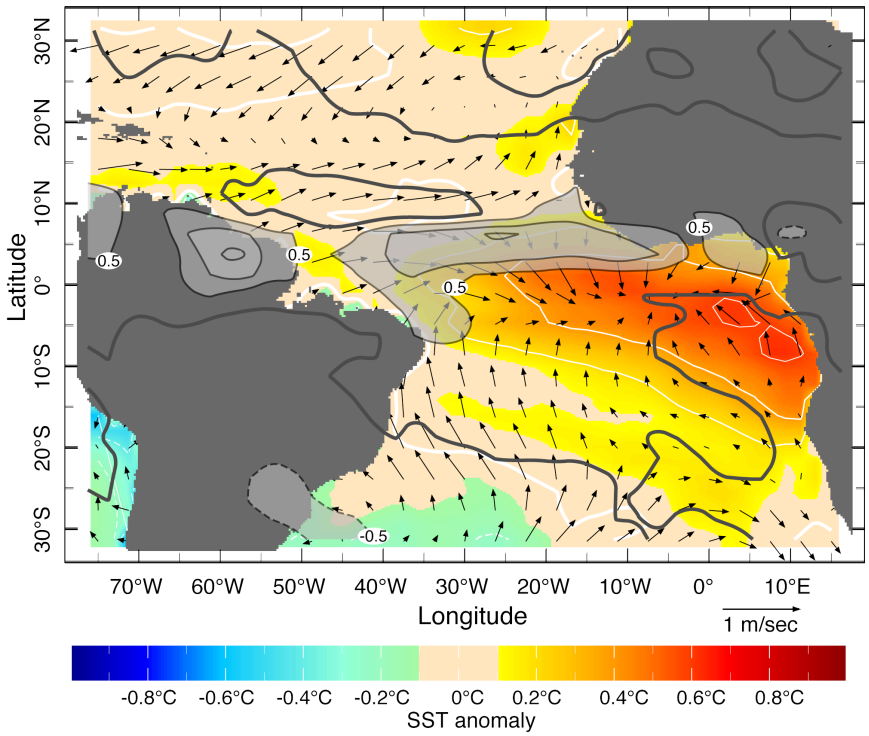

Figure 1.1.3b: Typical boreal summer variability in the tropical Atlantic region presented in terms of the first EOF (explains 23% of the variance) of the June-August rainfall from GPCP 1979-2001 (contours in mm/day). The June-August SST anomaly (colors, in °C & white contours, every 0.2°) and surface wind anomaly (vector, in m/sec) are determined through regression on the time series of the rainfall EOF.

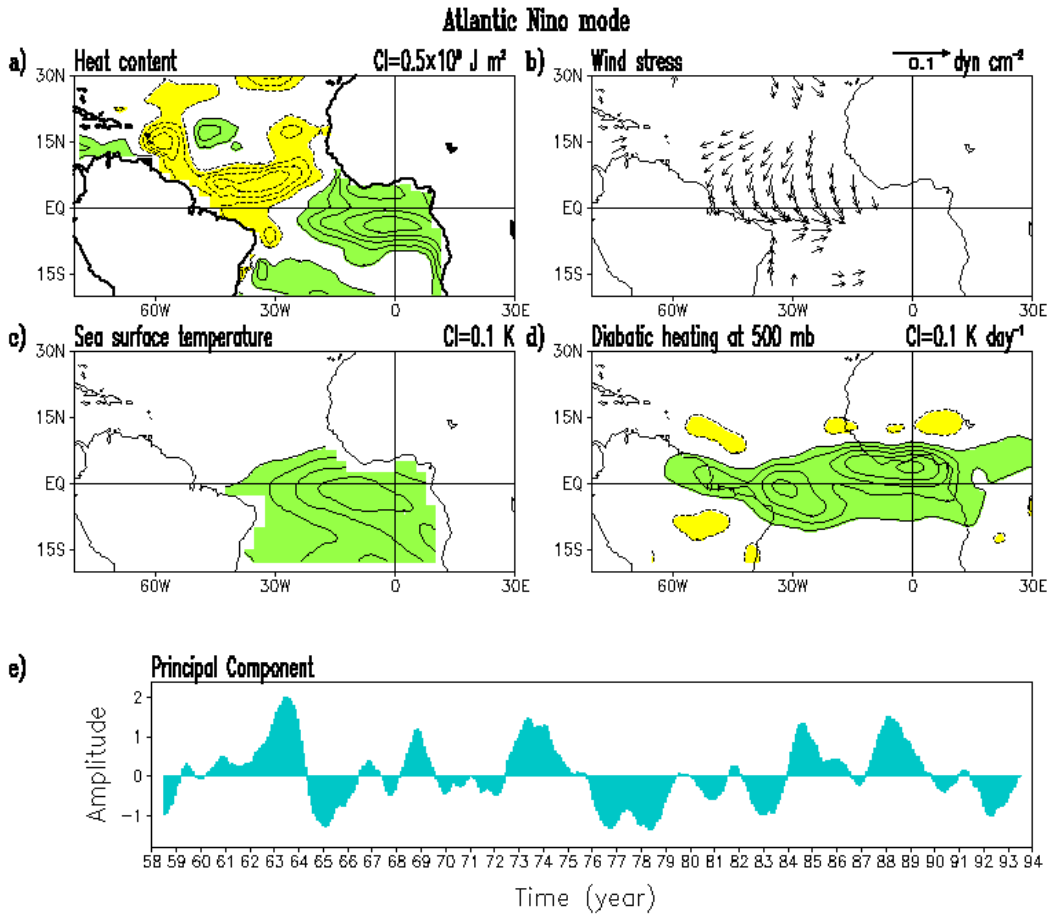

Figure 1.1.4 Anomalies associated with the Atlantic Nino principal component from a five-component rotated principal component analysis of observed heat content ($\times 10^8 Jm^2$, upper left), wind stress ($dyn\,cm^{-2}$, upper right), SST (^oC) middle left, diabatic heating at 500mb ($^oC\,dy^{-1}$, middle right) and the 12-month smoothed PC time series (bottom). From Ruiz-Barradas et al. (2000).

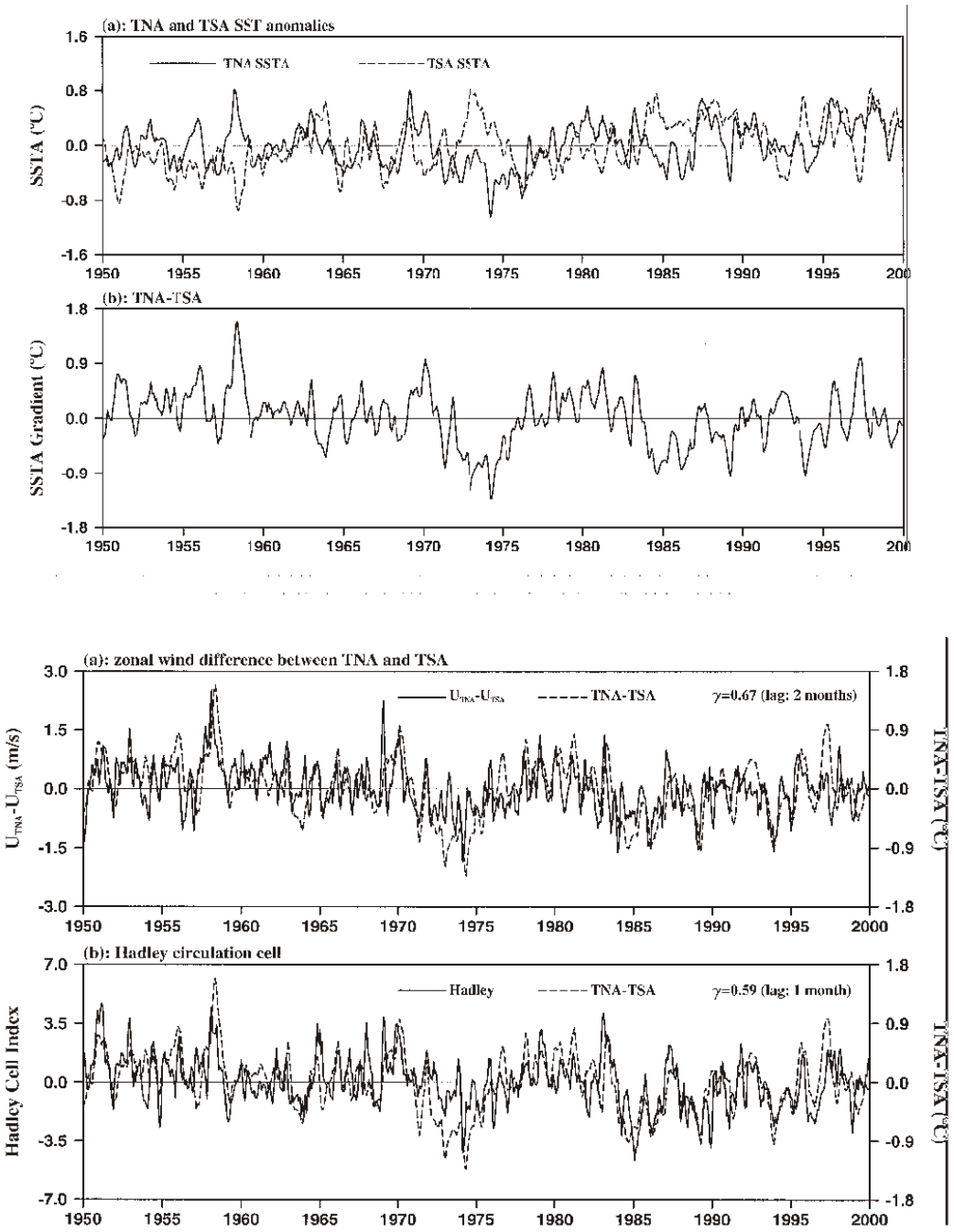

Figure 1.2.1 a) Time series of SST in NW (5-25N, 55-15W) and SE (0-20S, 30W-10E) tropical Atlantic and their difference; b) comparison of zonal wind anomaly and SST differences between NW and SE Atlantic and with Hadley cell Index of Wang (2001)

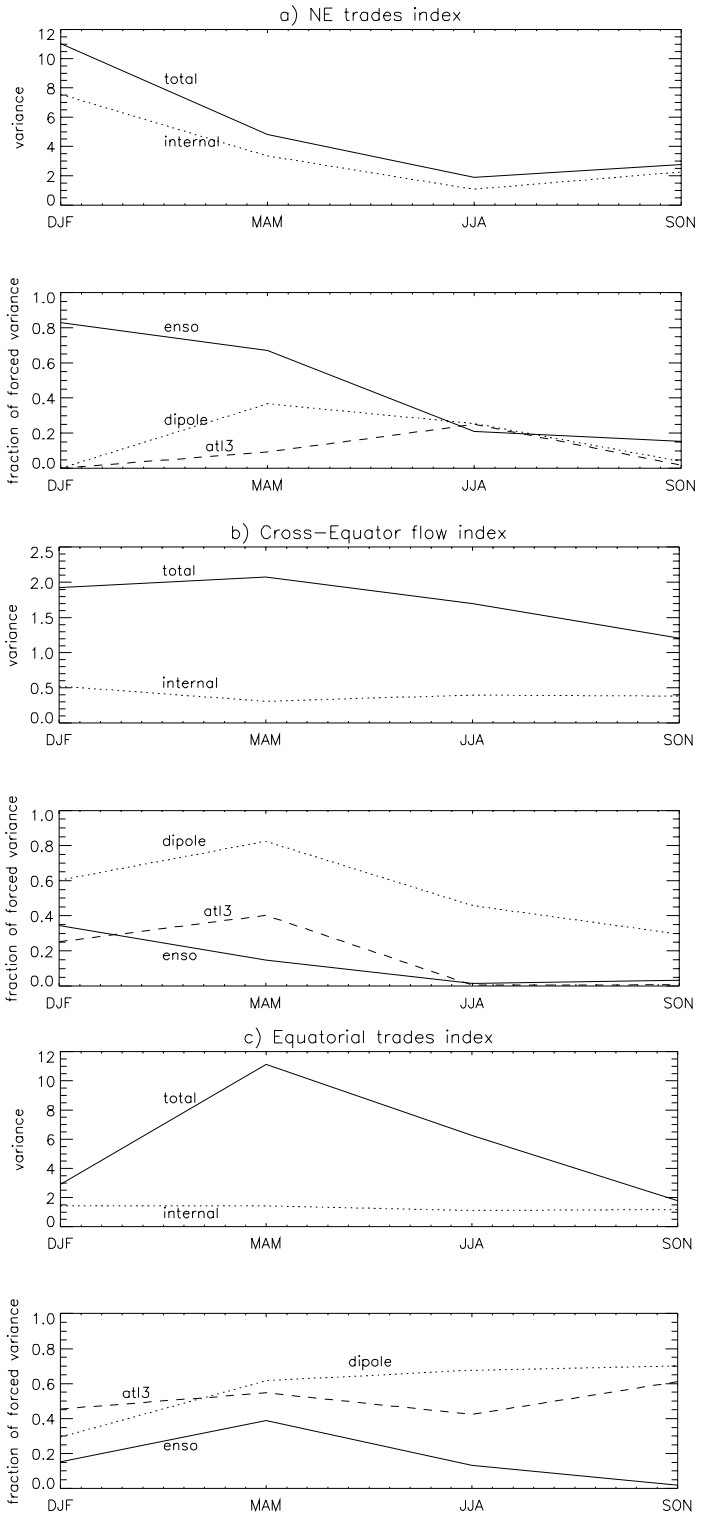

Figure 1.2.2 Seasonal variance partition between internal and SST-forced of three wind indices a) NE trades, b) cross-equatorial, c) zonal equatorial in an atmospheric model driven by observed SST; lower panels show fractions of SST-forced variance due to ENSO, Alt. equatorial SST (atl3) and SST dipole index (from Sutton et al., 2000)

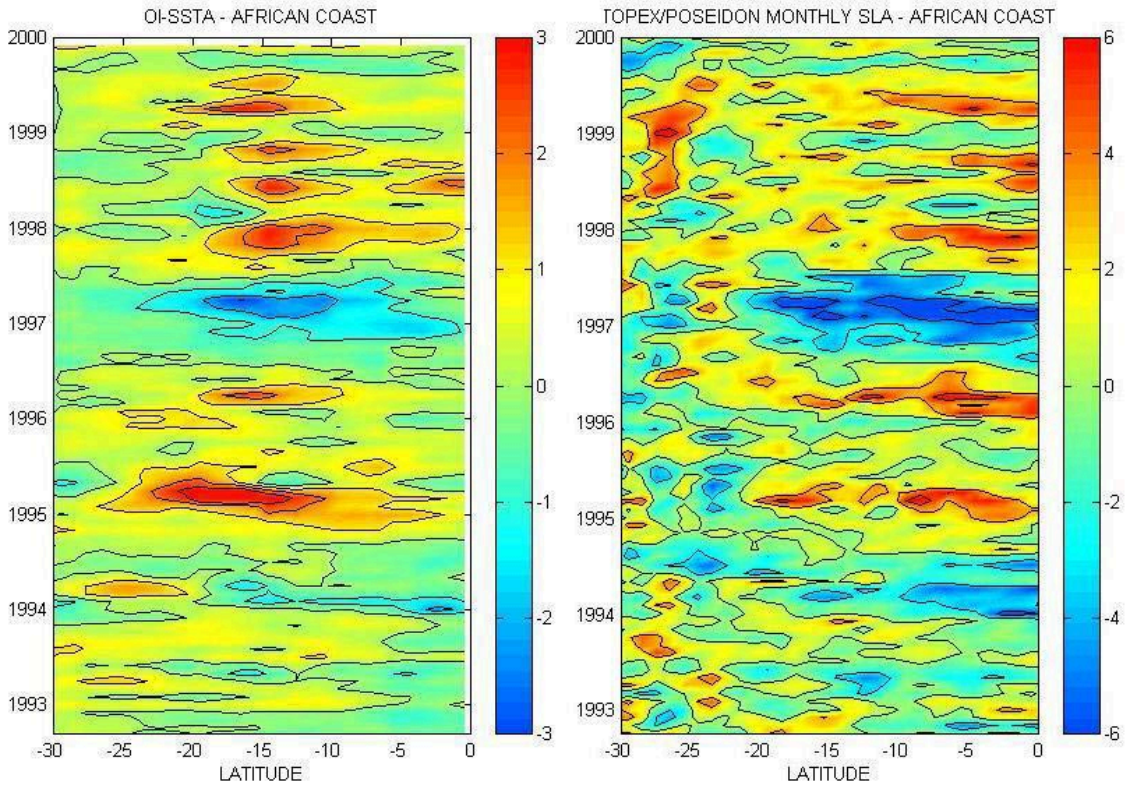

Figure 1.3.1 Sea surface temperature (right) and sea level (left) anomalies along the African coast from the equator to 30°S versus time (after Florenchie et al., 2003).

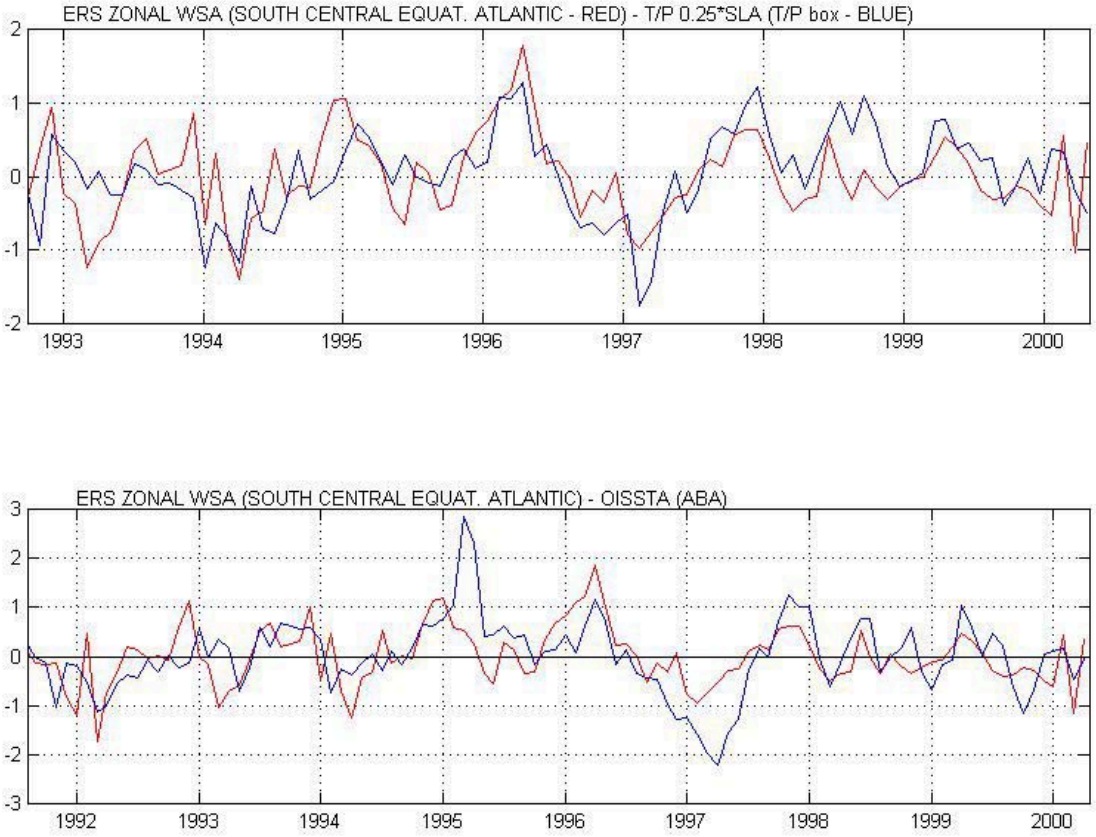

Figure 1.3.2 Time series of zonal WSA averaged south of the equator (between 5.5S and 0.5S) in the central basin from 29.5W to 9.5W and (a) SLA averaged over the Topex box and (b) OISSTA averaged over the ABA. After Florenchie *et al.,* 2003.

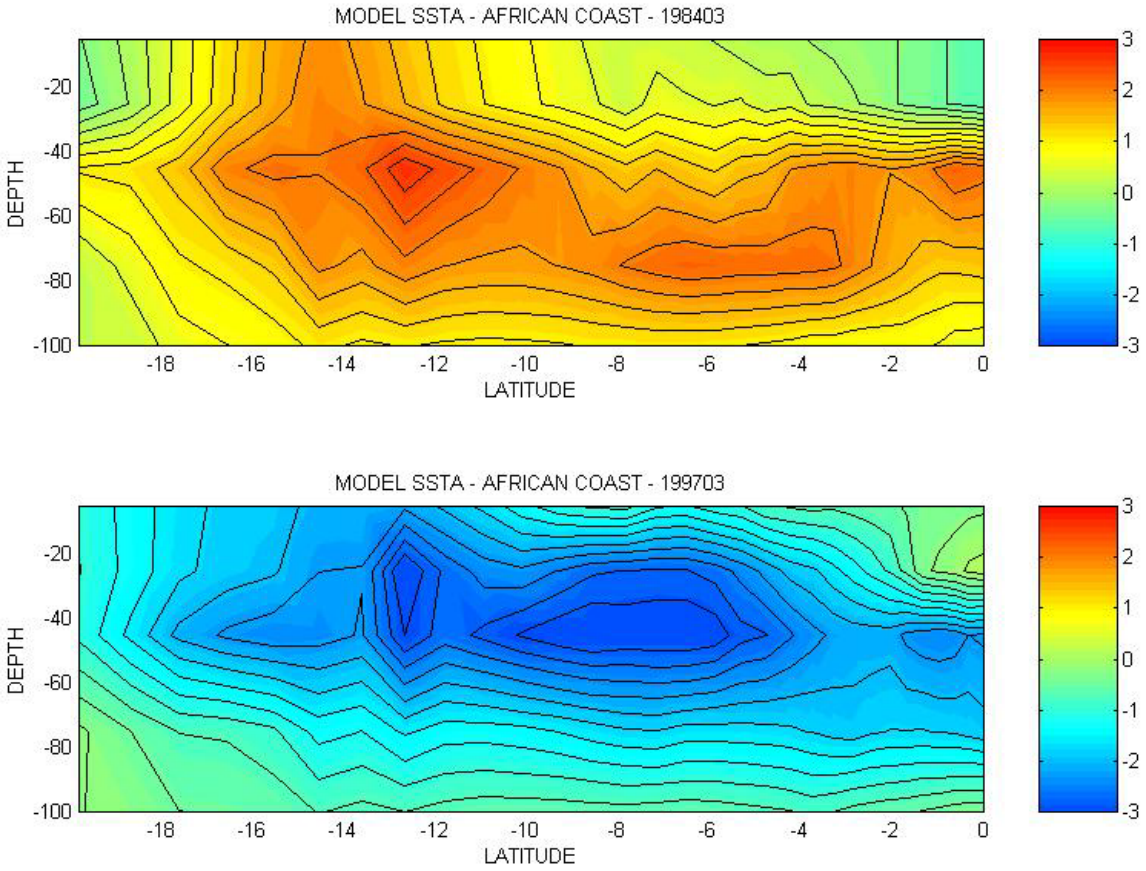

Figure 1.3.3a Subsurface propagation of warm and cold subsurface anomalies along the coast in March 1984 and 1997. After Florenchie *et al.* (2003)

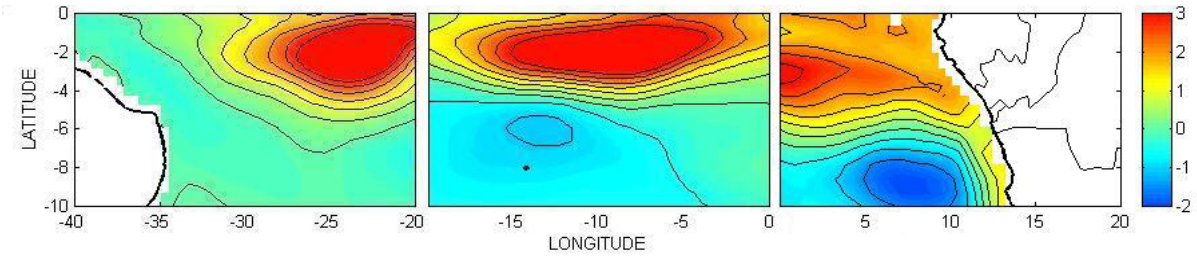

Figure 1.3.3b Time – depth evolution 1984 over 1 month, shoaling from 100 to 45 m across tropical Atlantic. After Florenchie *et al.* (2003).

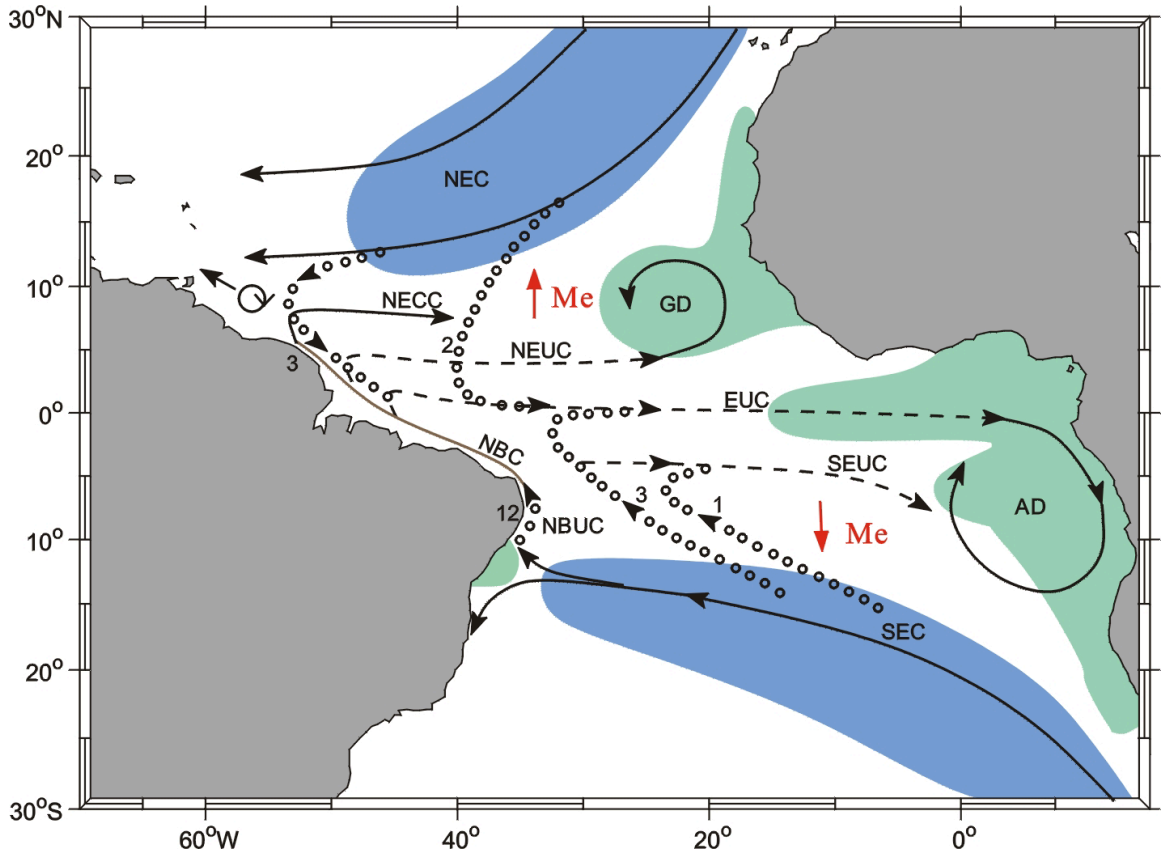

Figure 1.5.1 Schematic representation of the Atlantic STC circulation with subduction (blue), upwelling (green) zones and Ekman transports (red) that participate in the STC. For identified current branches participating in STC flows see Fig. 1.1.2. Interior equatorward thermocline pathways dotted, transport estimates marked for interior and western boundary pathways; see text for details.

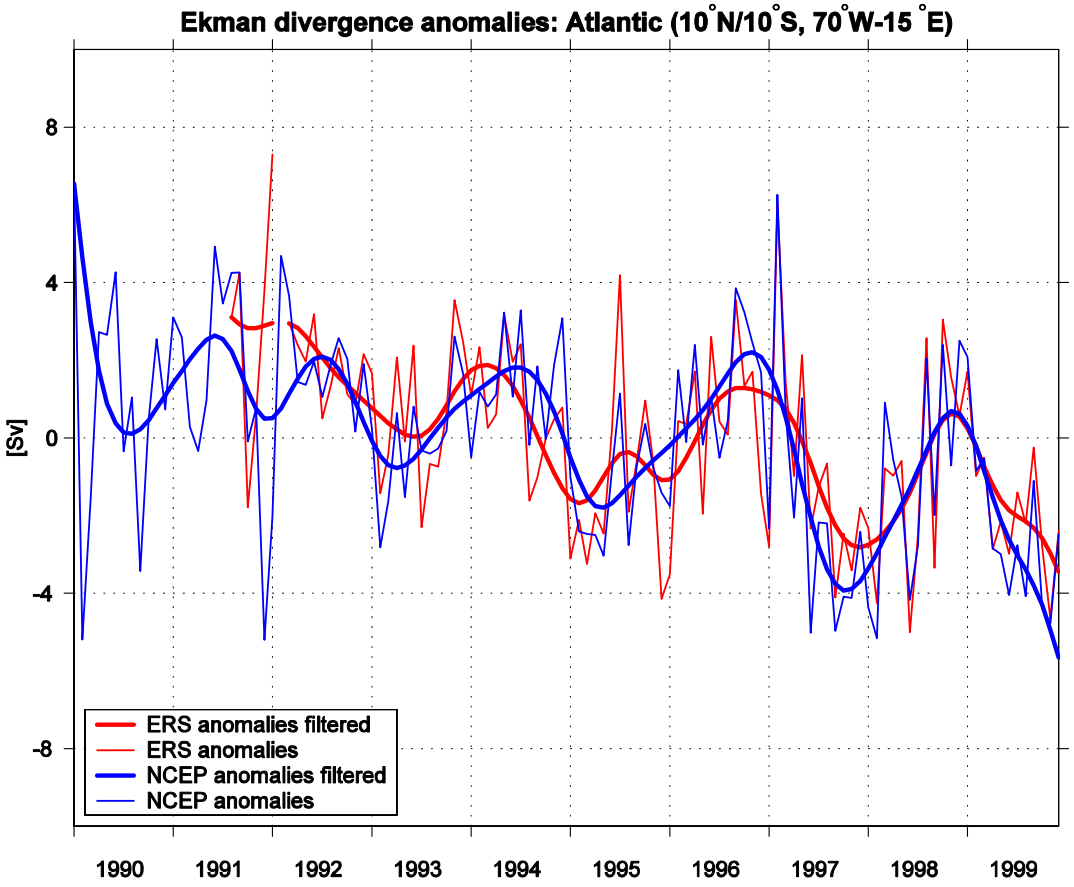

Figure 1.5.2 Time series of Ekman transport divergences across 10°N/10°S of monthly (thin) and lowpassed (heavy) anomalies from NCEP reanalysis (blue) and ERS-1/2 scatterometer (red) wind stresses.

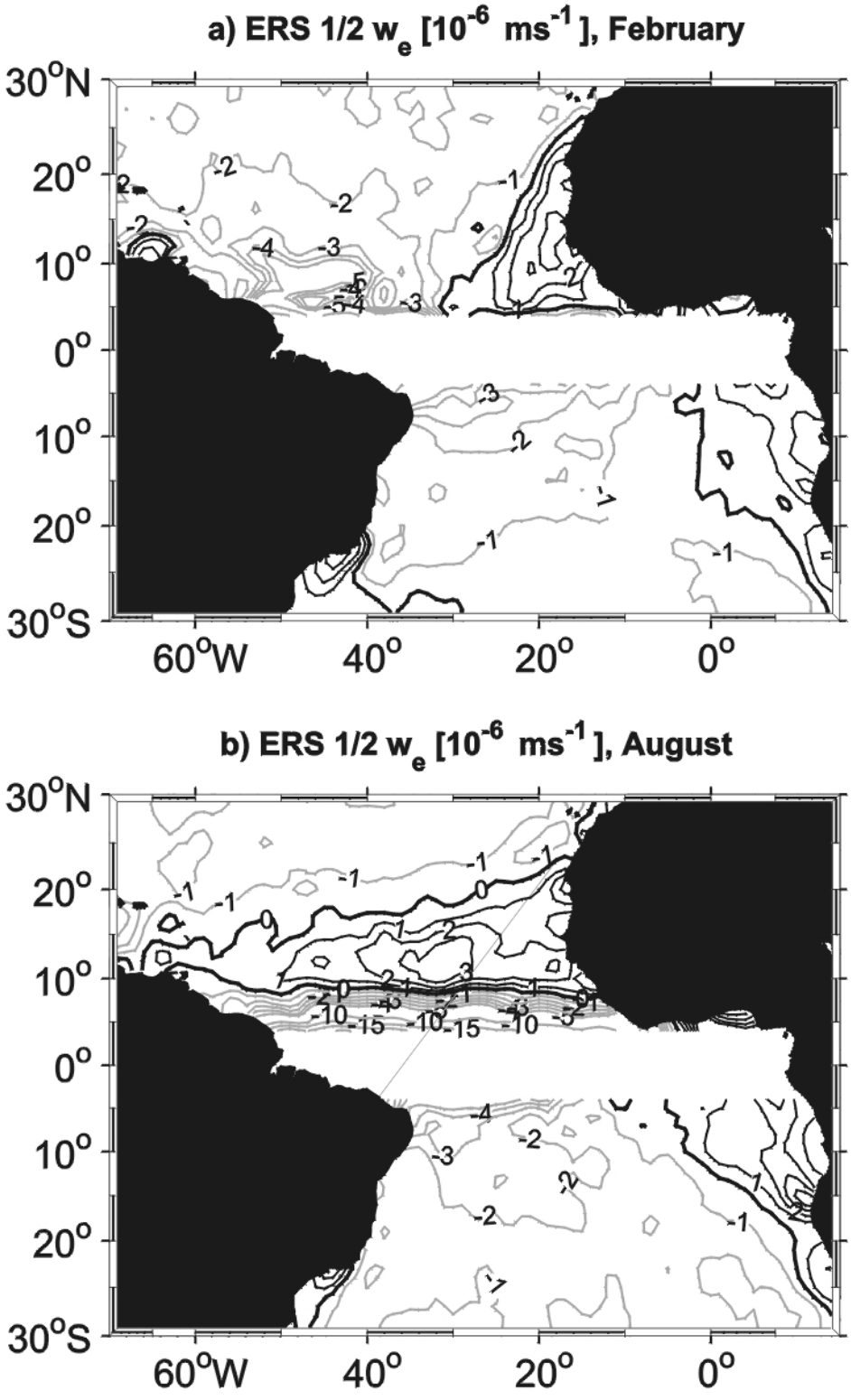

Figure 1.5.3 Ekman upwelling distribution for tropical Atlantic (outside $\pm 3^0$ latitude belt) from ERS-1/2 scatterometry wind stresses 1991-99 for a) February, b) August.

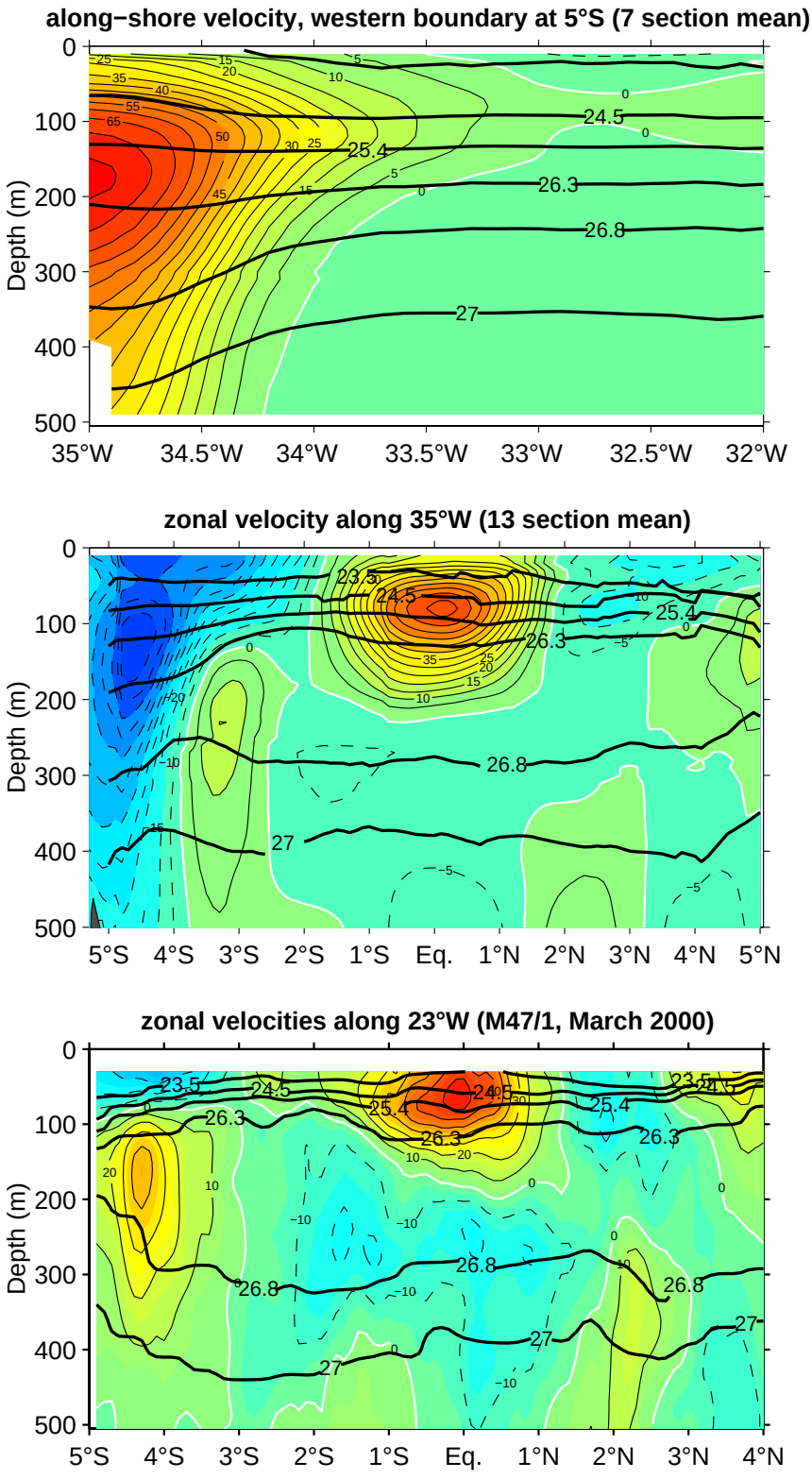

Figure 1.5.4 Mean zonal current distributions a) across the North Brazil Undercurrent at 5^0S (7 sections), b) across the zonal equatorial current system at 35^0W (11 sections) and at 23^0W (1 section); after Schott et al.,(2002, 2003).

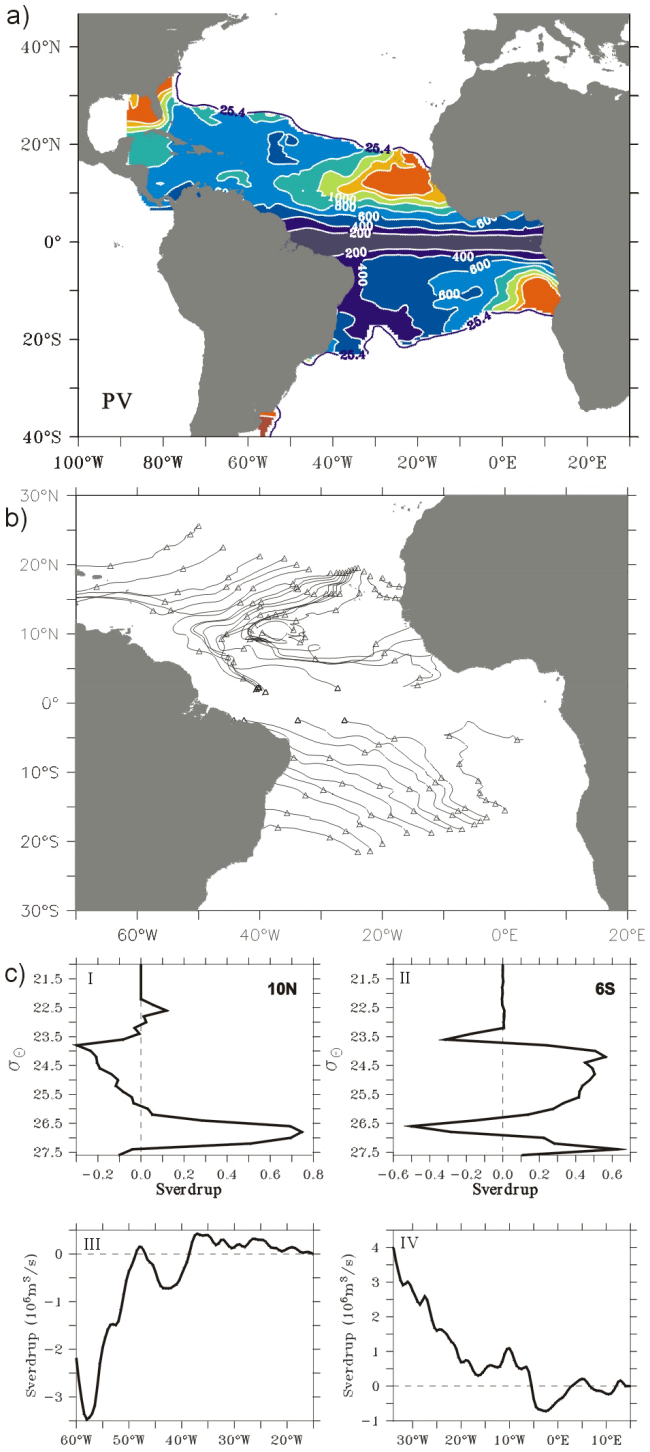

Figure 1.5.5 Distribution of potential vorticity and b) geostrophic currents on the isopycnal surface σ_θ = 25.4 kg·m^{-3} for the tropical Atlantic, based on climatological hydrographic data. c) Interior net meridional transports by density layers across 10^0N (African coast to 60W, left) and 6^0S (African coast to 35^0W, right). From Zhang et al. (2003).

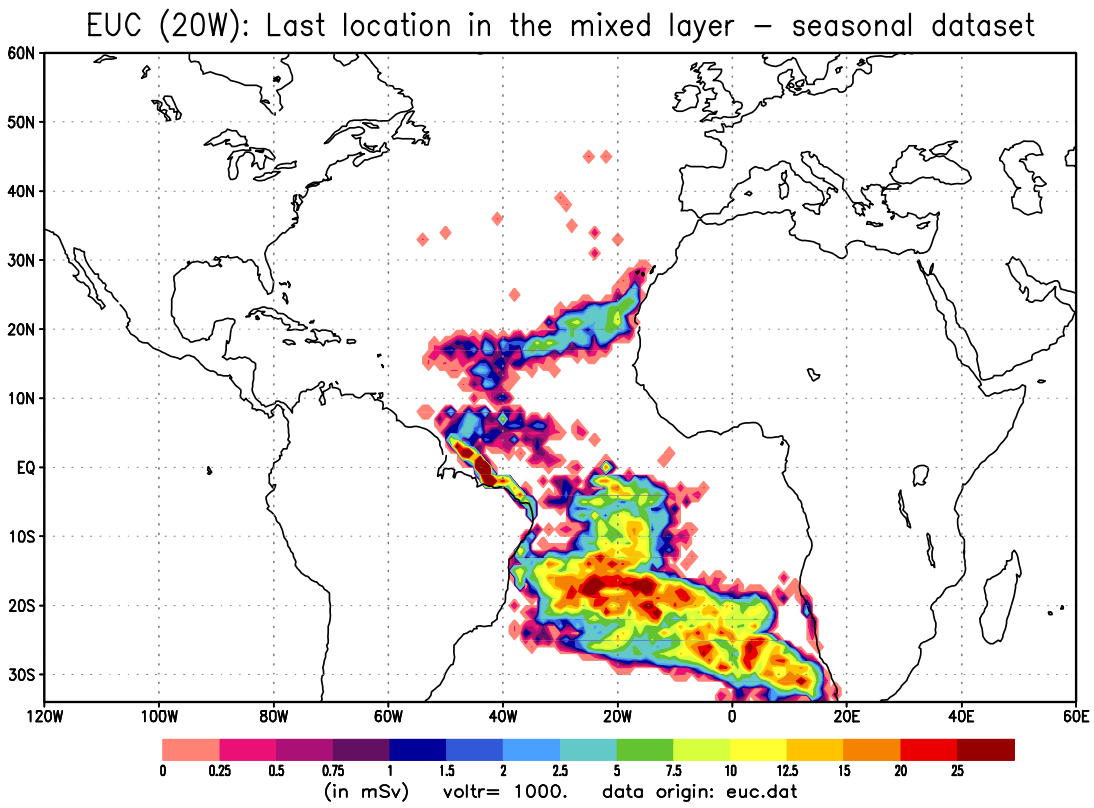

Figure 1.5.6 Subduction sites of water masses that ventilate the Equatorial Undercurrent at 20W (data from eddy-permitting OCCAM model, see Hazeleger et al. 2003a).

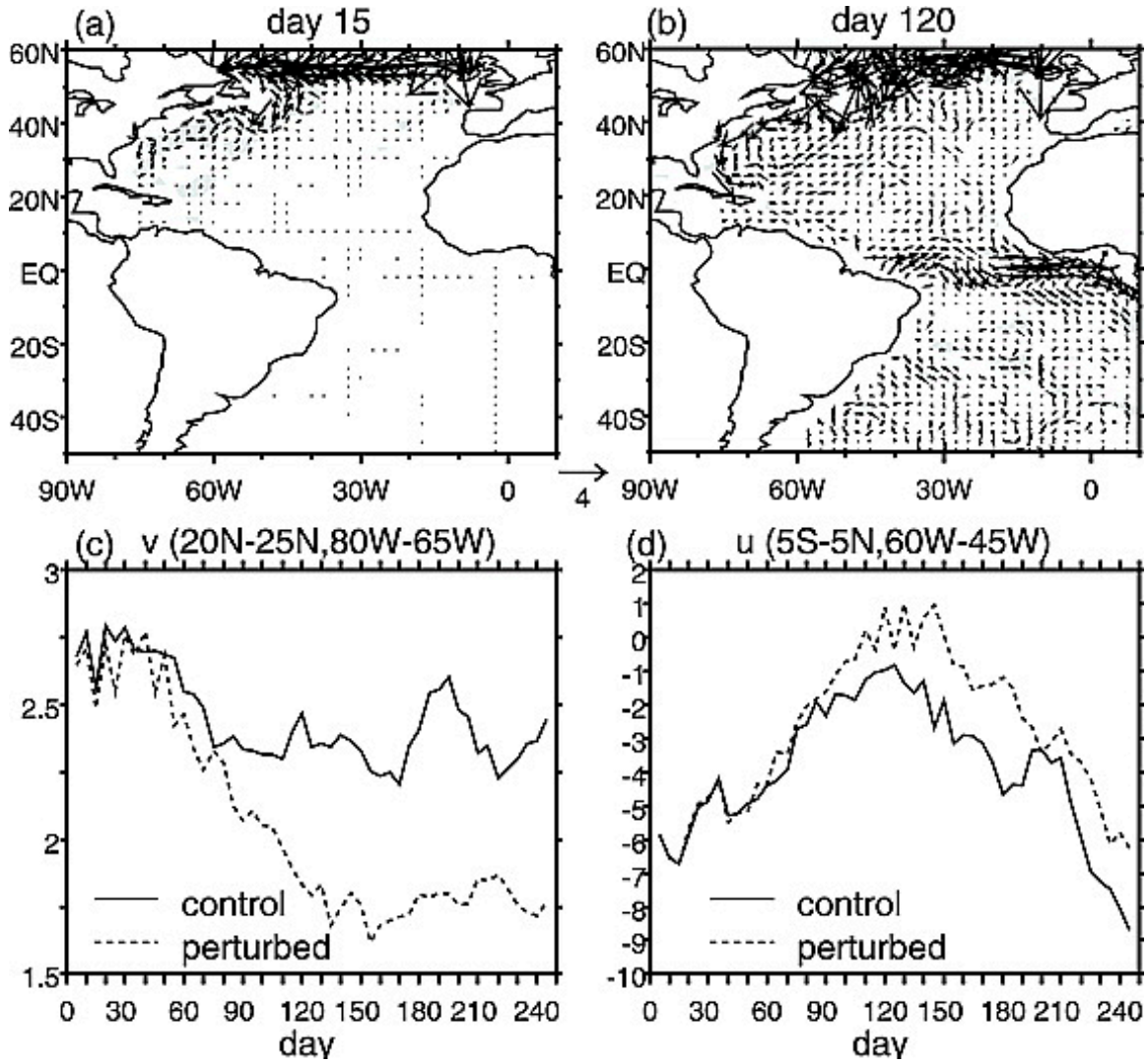

Figure 1.6.1 Upper ocean circulation anomlalies for (a) 15 days and (b) 120 days after perturbation of the MOC by introduction of a freshwater anomaly in the subpolar North Atlantic, and time variability of (c) meridional flow off Florida and (d) zonal currents in the equatorial Atlantic, between perturbed and control simulations (from Dong and Sutton, 2003).

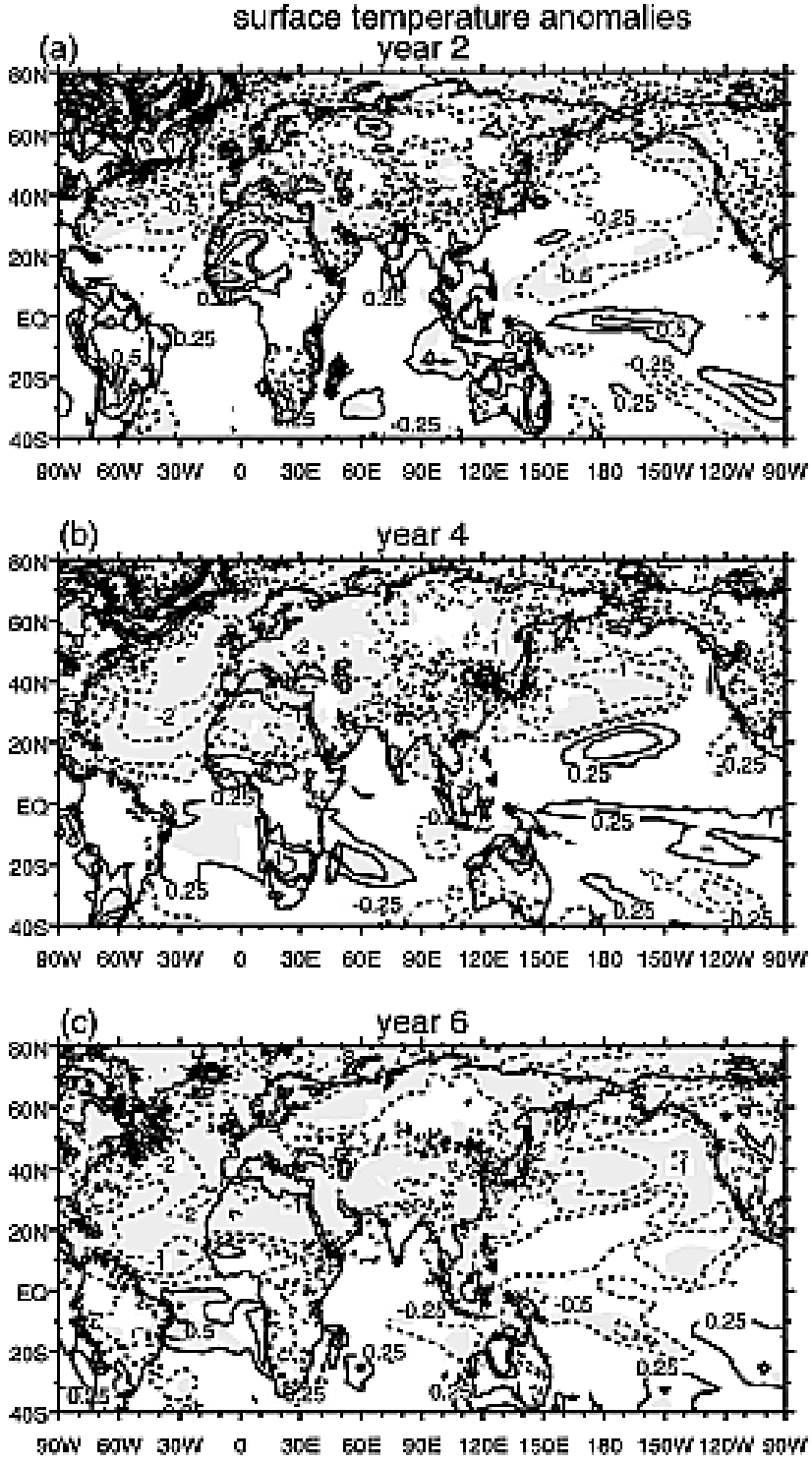

Figure 1.6.2 Global SST anomalies in years 2, 4, and 6 after reduction of the MOC by a subpolar freshwater anomaly (from Dong and Sutton, 2003).

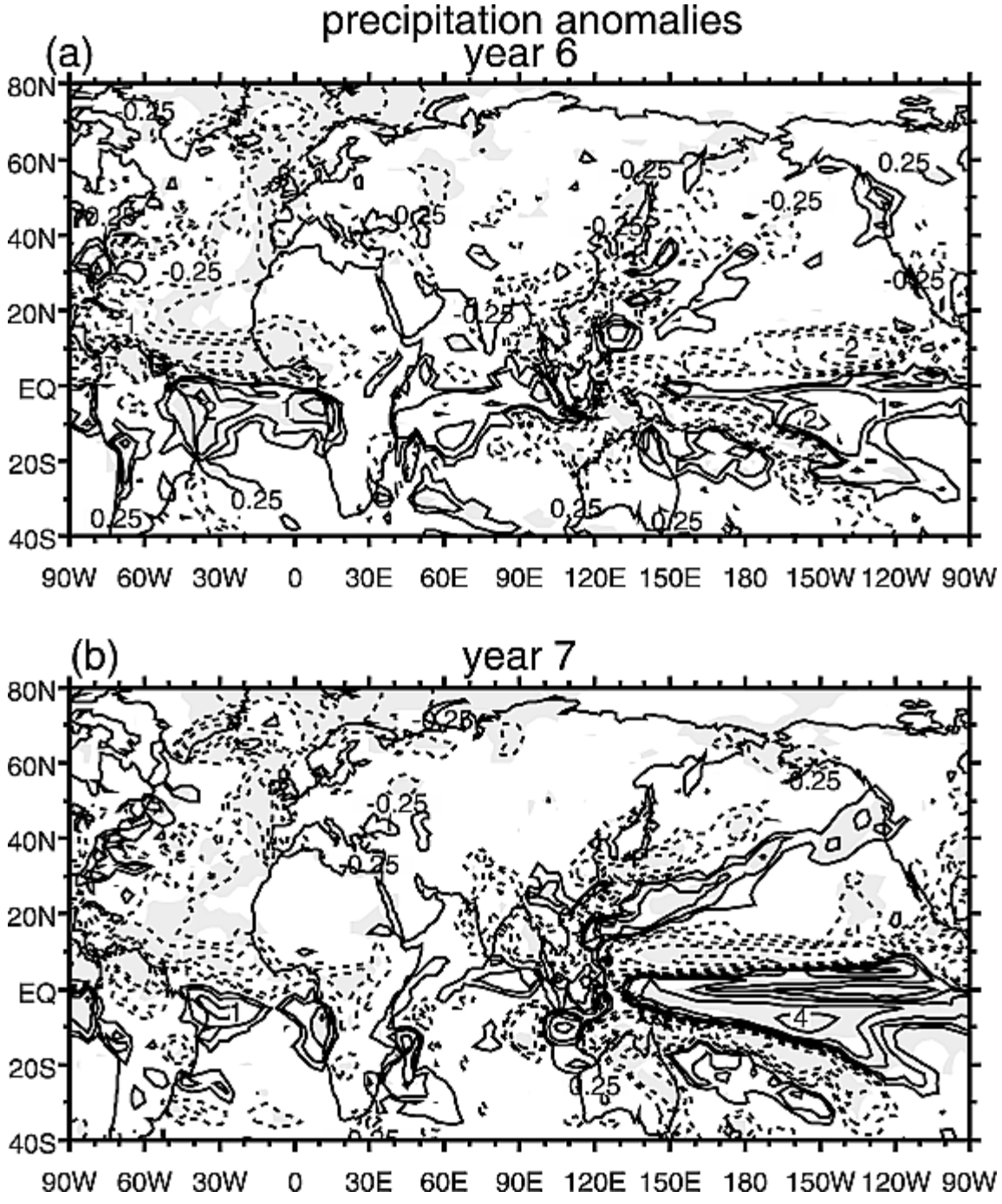

Figure 1.6.3 Global precipitation anomalies (mm/day) in (a) year 6 and (b) year 7 after a reduction in the MOC (from Dong and Sutton, 2003).

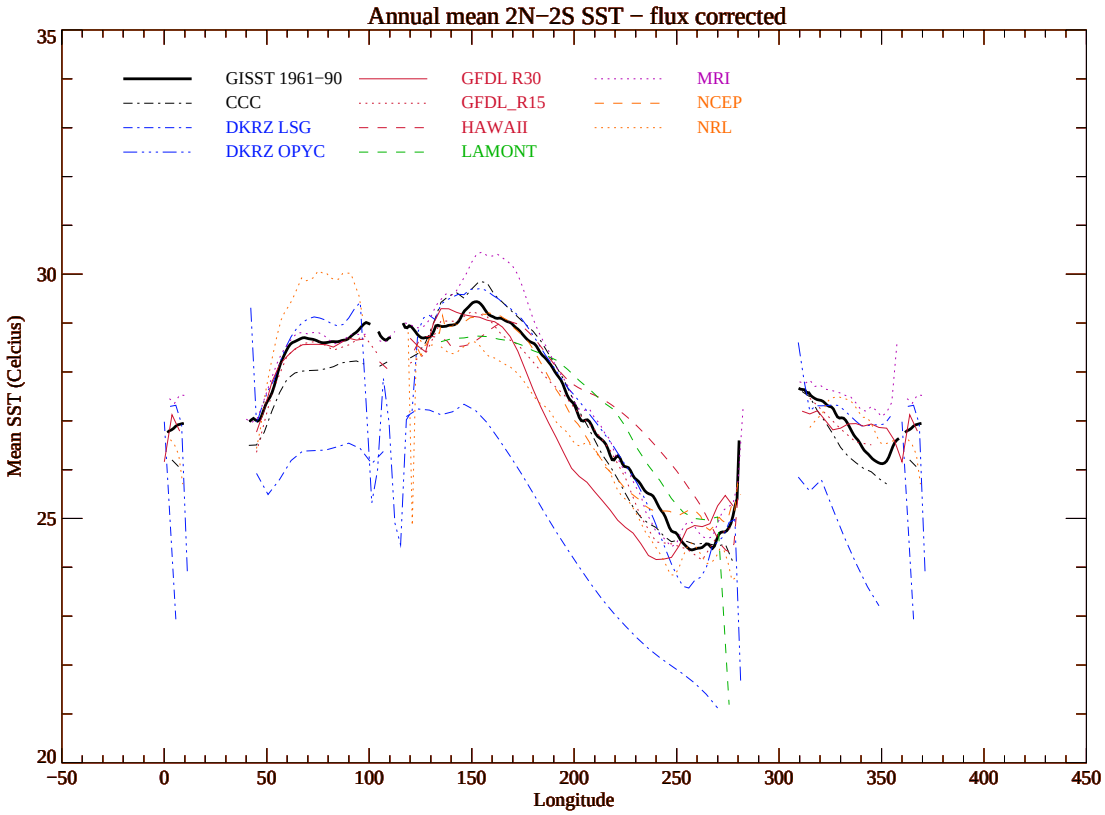

Figure 2.1 Annual mean SST zonal section for equatorial strip 2N-2S, as observed and for flux corrected CGCMs (compare with **Fig. 1.0.1** for non-flux corrected; with permission of M. Davey, see Davey et al 2002)

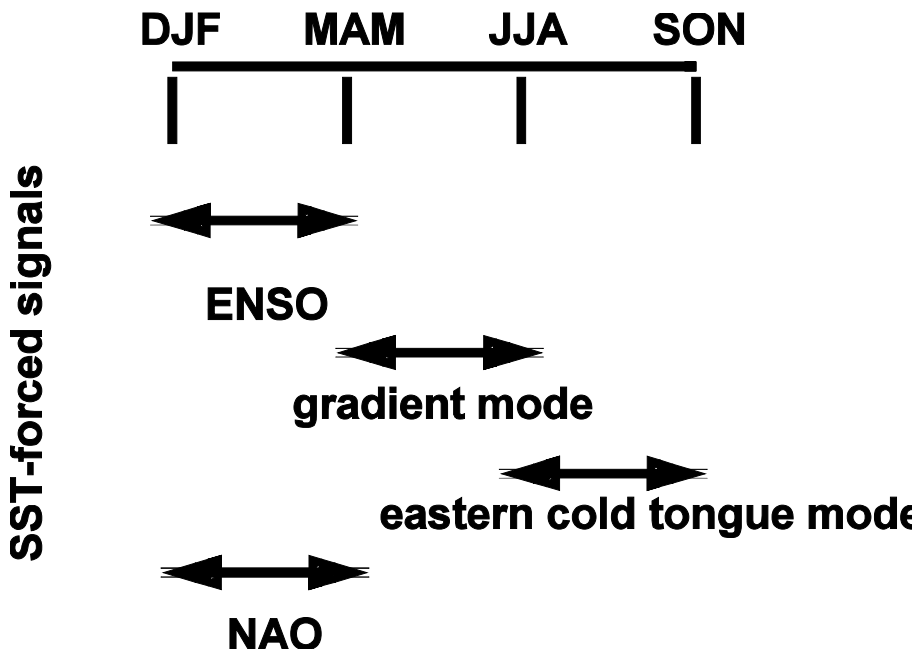

Figure 2.2 Summary of seasonality of the dominant elements of climate variability in the tropical Atlantic region (see Sutton et al. 2000).

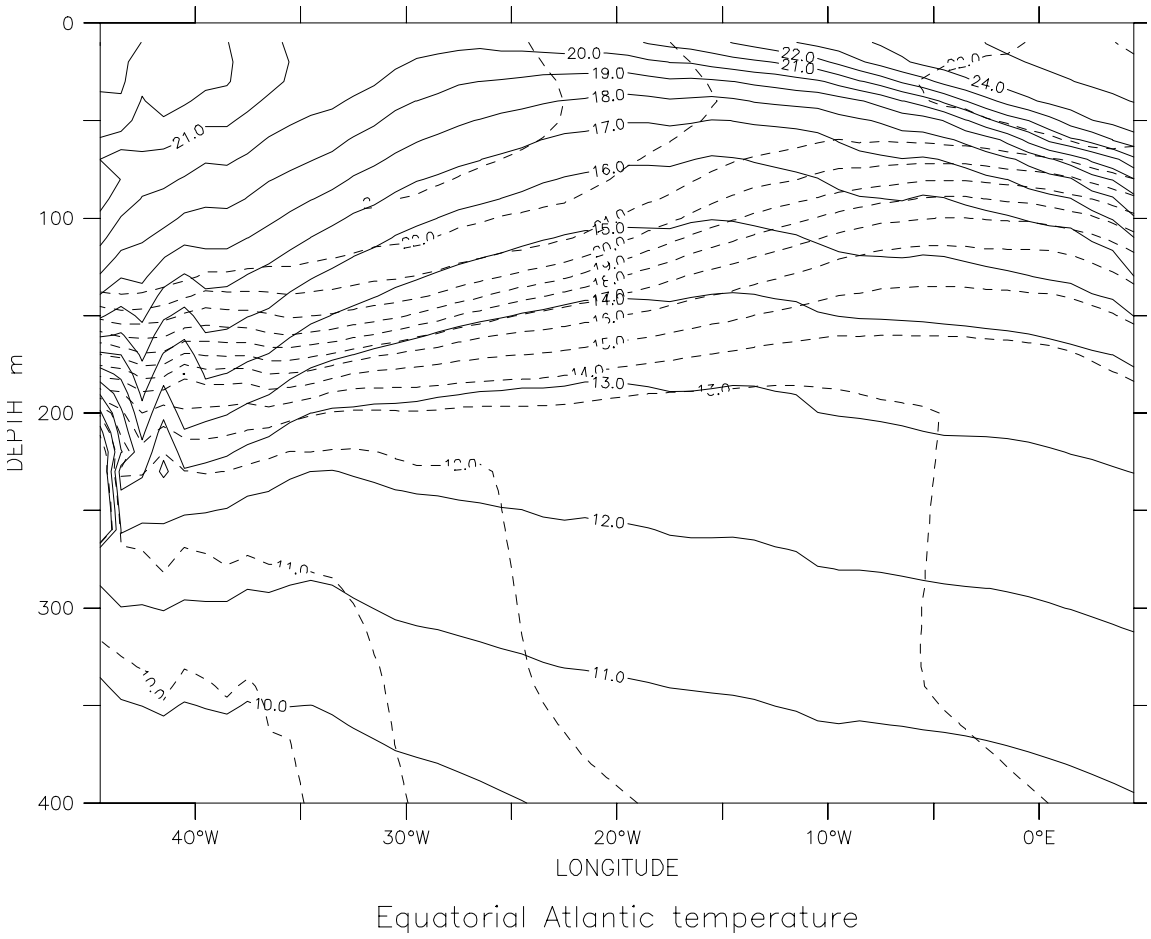

Figure 2.3 Temperature along the equator in a coupled primitive equation model (SPEEDO, see Hazeleger et al. 2003c). Continuous lines: with rather strong turbulent wind mixing coefficent in the Kraus-Turner mixed layer parameterization. Dashed lines: weak turbulent wind mixing coefficent.

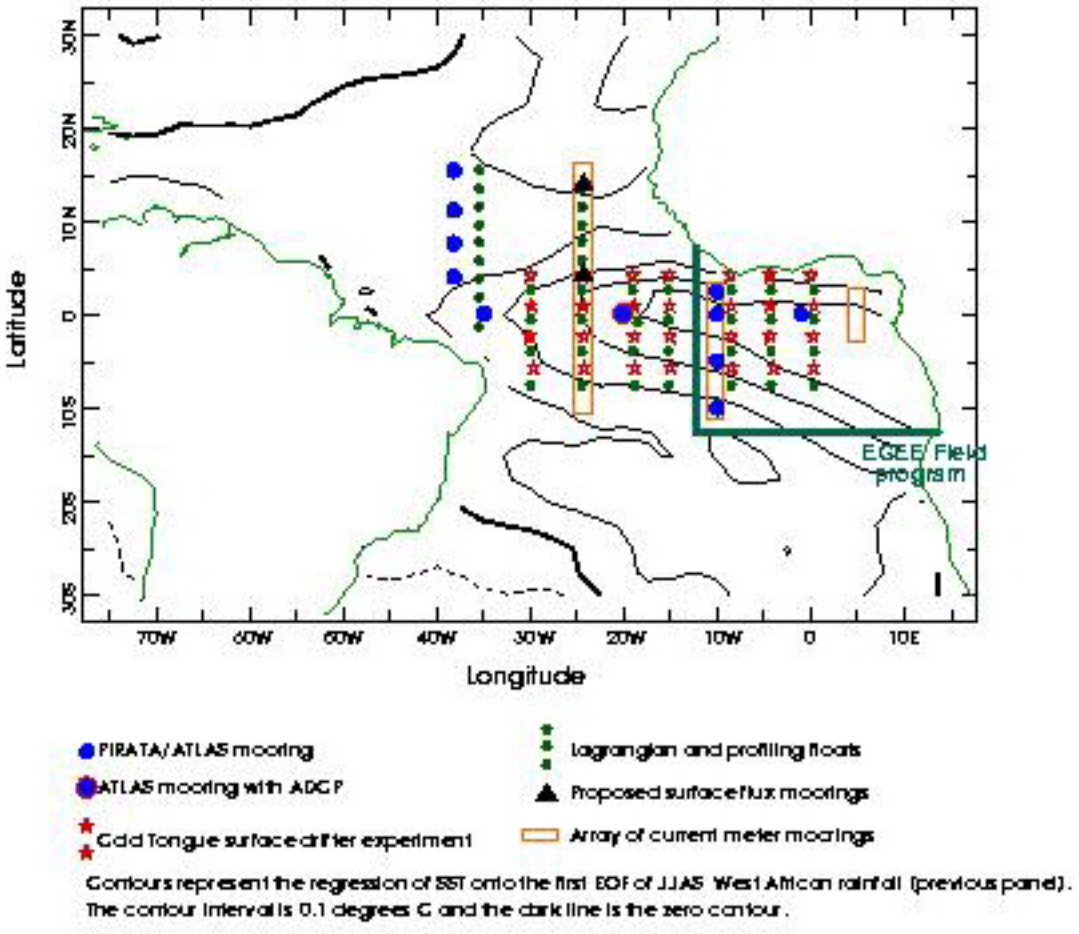

Figure 4.1 Schematic diagram of proposed observations for TACE with moored currentmeter arrays, flux moorings, drifters and floats; also shown is regression of SST on 1st EOF of July-Sept. W.African rainfall.

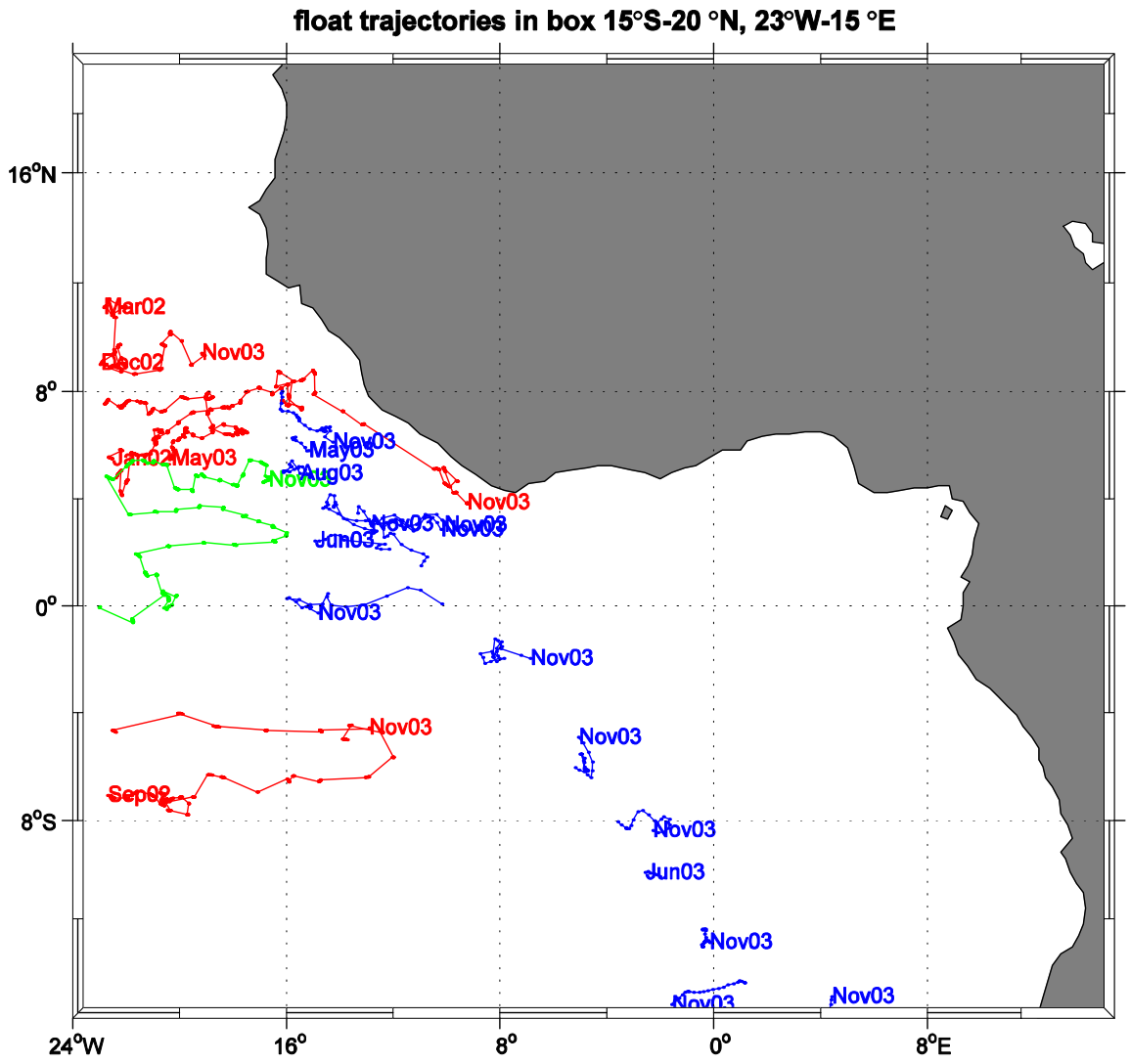

Figure 4.2 Trajectories of profiling floats in the TACE region at shallow STC levels and deep, Nov. 2003 (http://www.coriolis.eu.org).

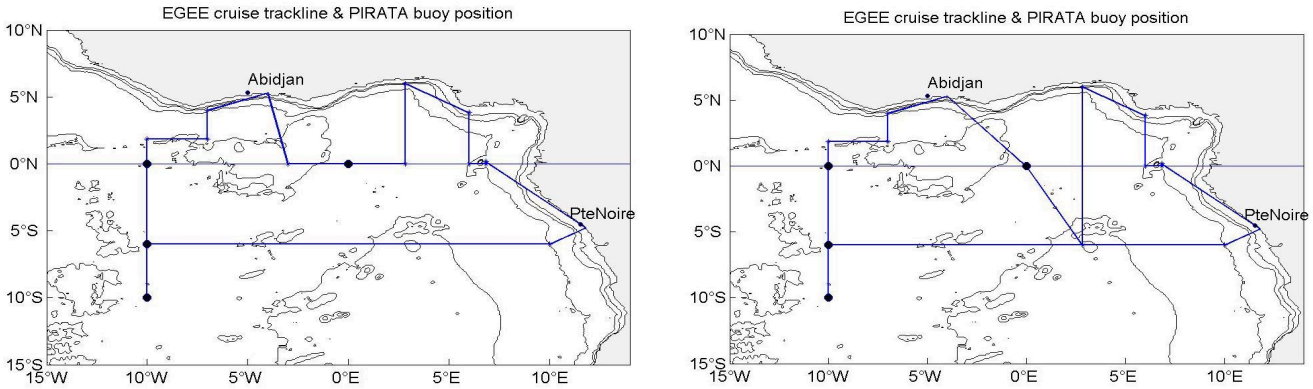

Figure 5.1 proposed EGEE alternative repeat cruise tracklines, including a meridional section around 3°E, south of Benin and of the "CATCH" area. The option on the r.h.s. is slightly more expensive in vessel time. The position of the four ATLAS buoys of the PIRATA network are also represented (black dots). The passing through the 10°S-10°W buoy will depend upon the PIRATA program demand (visit of the buoy at least once a year), but the zonal section at 6°S could be shifted at 10°S.

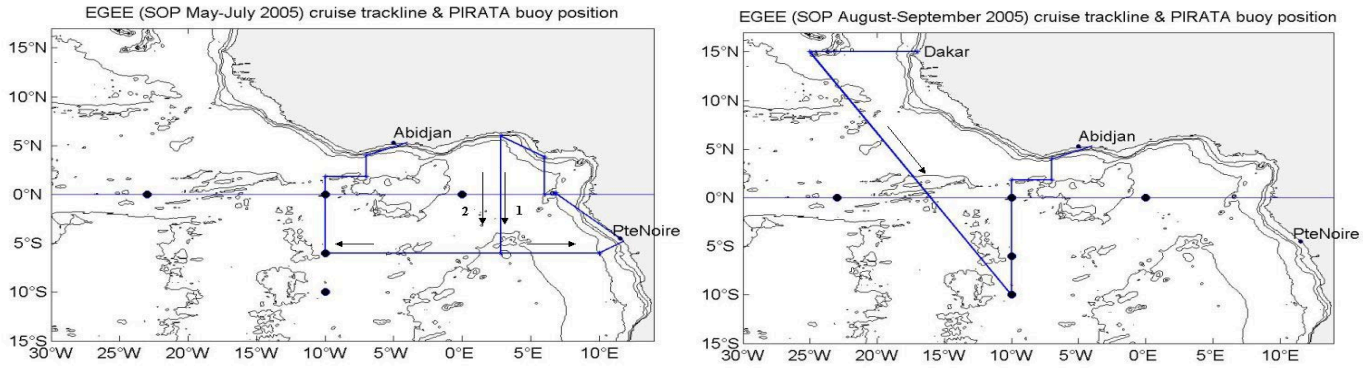

Figure 5.2 proposed EGEE cruises tracklines in 2006, during the AMMA SOP 1 (May-July, on the left) and SOP 3 (end of August-September, on the right). The position of the four ATLAS buoys of the PIRATA network are also represented (black dots). The passing through the 10°S-10°W buoy will depend upon the PIRATA program demand (visit of the buoy at least once a year), but the zonal section at 6°S could be shifted to 10°S.